International Journal of Innovative Computing, Information and Control
Volume **9**, Number **2**, February **2013**

ICIC International ©2013 ISSN 1349-4198
pp. 875–901

A STUDY OF NEGATIVE SELECTION ALGORITHM-BASED MOTOR FAULT DETECTION AND DIAGNOSIS

Xiao-Zhi Gao[1], He Xu[2], Xiaolei Wang[1] and Kai Zenger[1]

[1]Department of Automation and Systems Technology
School of Electrical Engineering
Aalto University
Aalto 00076, Finland
{xiao-zhi.gao; xiaolei.wang; kai.zenger}@aalto.fi

[2]College of Mechanical and Electrical Engineering
Harbin Engineering University
No. 145, Nantong Street, Nangang District, Harbin 150001, P. R. China
xuhe@hrbeu.edu.cn

Received December 2011; revised April 2012

Abstract. *In this paper, we present a comprehensive study of the Negative Selection Algorithm (NSA)-based motor fault detection and diagnosis. The NSA only needs the feature signals of the healthy motors for generating the motor fault detectors. Different from the conventional fault detection approaches, no prior knowledge of the motor fault types is assumed to be known beforehand. Based on the motor fault detection results, the NSA can be further applied for the fault diagnosis. The applicability of our motor fault detection and diagnosis method is examined using the Fisher's iris data classification and three real-world motor fault detection and diagnosis problems in computer simulations.*
Keywords: Artificial Immune Systems (AIS), Negative Selection Algorithm (NSA), Fault detection, Fault diagnosis, Motors, Electrical machines, Mobile robots

1. **Introduction.** The Artificial Immune Systems (AIS) are inspired by the principles of the natural immune systems [1], and are considered as one kind of popular computational intelligence methods [2]. The AIS have the distinguishing features of pattern recognition, anomaly detection, optimization, data analysis, machine learning, etc. They have drawn growing interests from researchers with various backgrounds during the past decade [3,4]. The Negative Selection Algorithm (NSA) is an important AIS method, which is based on the theory of the maturation of the T cells and self/nonself discrimination in the biological immune systems. It was firstly developed by Forrest *et al.* in 1994 for the real-time detection of computer viruses [5], and has also been widely applied in such diverse engineering areas as communication network security [6], milling tool breakage monitoring [7], and aircraft fault detection [8].

This paper first proposes an NSA-based motor fault detection scheme, in which the detectors are generated from only the feature signals of the healthy motors. It does not need any prior information of the faults to be detected. Furthermore, based on the fault detection results, we employ the NSA to deal with the motor fault diagnosis problem. The validity of the proposed motor fault detection and diagnosis approach is also verified using numerical simulations of several practical problems.

The remaining part of this paper is organized as follows. The basic principles of the NSA are presented and explained in Section 2. We propose and discuss the NSA-based motor fault detection scheme in Section 3. A new motor fault diagnosis system using the NSA is further built up in Section 4. Section 5 demonstrates the simulation results of

our motor fault detection and diagnosis method with four case study examples. Finally, a few conclusions and remarks are drawn in Section 6.

2. **Principles of Negative Selection Algorithm (NSA).** The natural immune system is an efficient self-defense system that can protect the human body from being affected by foreign antigens or pathogens [1]. One of its most important functions is pattern recognition and classification. In other words, the biological immune system is well capable of distinguishing the self, i.e., normal cells, from the nonself, such as bacteria, viruses and cancer cells. This interesting capability is implemented mainly by two types of lymphocytes: B cells and T cells. Both the B cells and T cells are produced in the bone marrow. However, for the T cells, they must pass through a so-called *negative* selection procedure in the thymus thereafter. Only those that do not match the self proteins of the body will be released out to circulate, while the remaining others are eventually destroyed. The censoring of the T cells can actually prevent our immune system from attacking the body's own proteins.

Forrest *et al.* firstly propose the Negative Selection Algorithm (NSA) [5] to mimic the aforementioned T cells maturation mechanism of the biological immune system, as shown in Figure 1. This approach can be conceptually described as follows [9]. Defining the self, we first collect a data set containing some representative self samples. Next, the candidate detectors are *randomly* generated, and compared with the self set. Note, like the above negative selection of the T cells, only those detectors that do not match any element of the self sample set are retained. To put it into more details, let $[x_1, x_2, \cdots, x_L]$ and $[w_1, w_2, \cdots, w_L]$ denote a self sample and a candidate detector, respectively, where L is their common order. The matching degree d between $[x_1, x_2, \cdots, x_L]$ and $[w_1, w_2, \cdots, w_L]$ can be calculated based on the Euclidean distance:

$$d = \sqrt{\sum_{i=1}^{L} (x_i - w_i)^2}. \tag{1}$$

d is then compared with a preset threshold λ, and the detector matching error E is obtained:

$$E = d - \lambda. \tag{2}$$

If $E > 0$, detector $[w_1, w_2, \cdots, w_L]$ fails to match self sample $[x_1, x_2, \cdots, x_L]$, and if $[w_1, w_2, \cdots, w_L]$ does not match all the self samples, it will be included in the detector set.

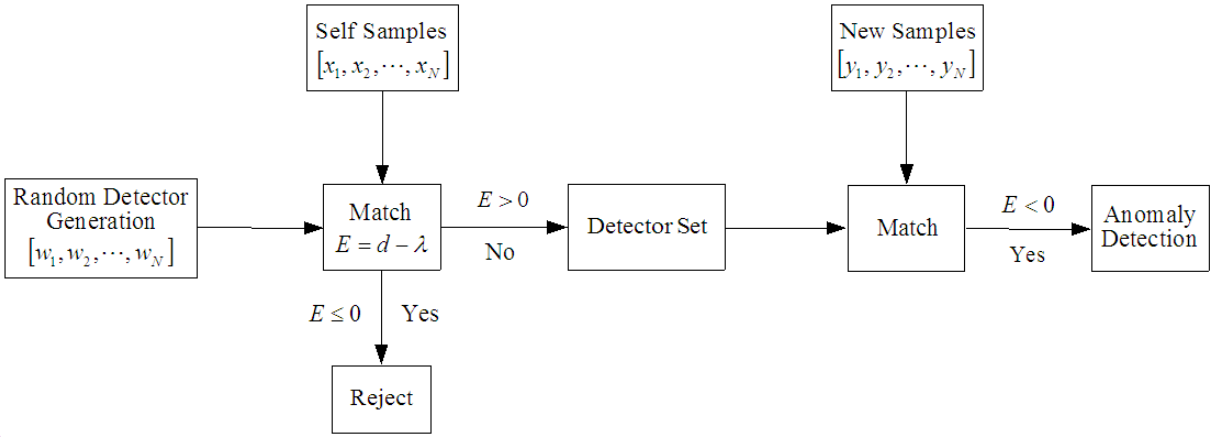

FIGURE 1. Negative Selection Algorithm (NSA)

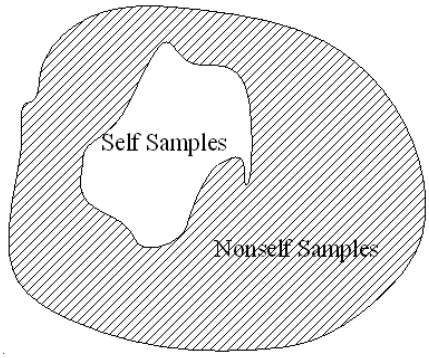

FIGURE 2. Self and nonself samples

On the other hand, if $E \leq 0$, we consider that $[w_1, w_2, \cdots, w_L]$ matches $[x_1, x_2, \cdots, x_L]$, and it is, thus, rejected. After a certain number of qualified detectors are generated by such a negative selection procedure, they are used to detect the anomaly (nonself samples) in the fresh data. That is, when $[w_1, w_2, \cdots, w_L]$ matches a new sample $[y_1, y_2, \cdots, y_N]$, the existing anomaly can be detected. The general relationship between the self and nonself samples is illustrated in Figure 2.

The original NSA has been shown to have some drawbacks in handling real-world problems [10]. Thus, during the recent years, various types of the modified NSA have been studied to yield improved performances. For example, Ji and Dasgupta propose a variant NSA on the basis of variable-sized detectors (V-detectors) [11,12]. In the V-detectors NSA, each self sample has a vicinity (self radius). A V-detector is randomly positioned, and its radius is dynamically changed until it reaches the margin of the nearest self sample. Stibor *et al.* compare the V-detectors NSA with the Bayesian classification method and one-class Support Vector Machine (SVM) in the anomaly detection [13]. The performance of the V-detectors NSA is discovered to be sensitive to several parameters, such as the self radius. In summary, the past years have witnessed the great successes of employing the NSA in anomaly detection, computer networks security, fault detection, etc.

3. **Negative Selection Algorithm (NSA) in Motor Fault Detection.** Fault detection/diagnosis methods are indeed crucial in modern industry to ensure the normal working conditions of plants, such as electrical machines, motors, and processes [14-16]. Especially, those motor faults may result in serious performance degradation and even eventual system failures, if not properly detected as well as handled. Therefore, motor status monitoring and fault detection are important but demanding topics in the electrical engineering field. Generally, we can consider the anomaly in the feature signals acquired from the faulty motors is caused by incipient faults. Hence, fault detection is converted to a representative problem of anomaly detection [17], i.e., self/nonself discrimination, in the characteristic time series, which can be handled by utilizing the NSA. A few variants of the NSA with applications in motor fault detection have also been proposed and studied by the authors of the present papers [18-21]. Similar to Figure 2, Figure 3 shows the normal, abnormal, and faulty feature signals of the motors. Note that the faulty feature signal is only a subset of the abnormal one.

In this section, we present an NSA-based motor fault detection scheme, as illustrated in Figure 4. Our approach consists of three main stages. Firstly, the feature signals of the healthy motors are sampled and preprocessed. They are usually split into non-overlapping or overlapping windows in the signal preprocessing unit, denoted by $[x_1, x_2, \cdots, x_N]$, as

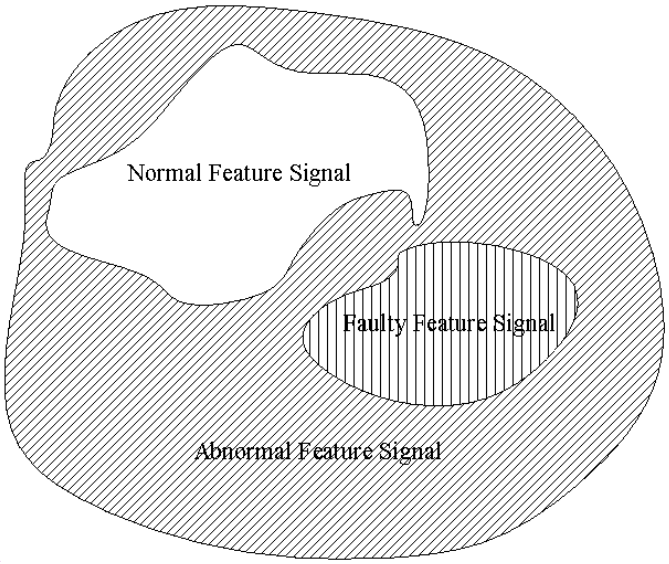

FIGURE 3. Normal, abnormal and faulty feature signals of motors

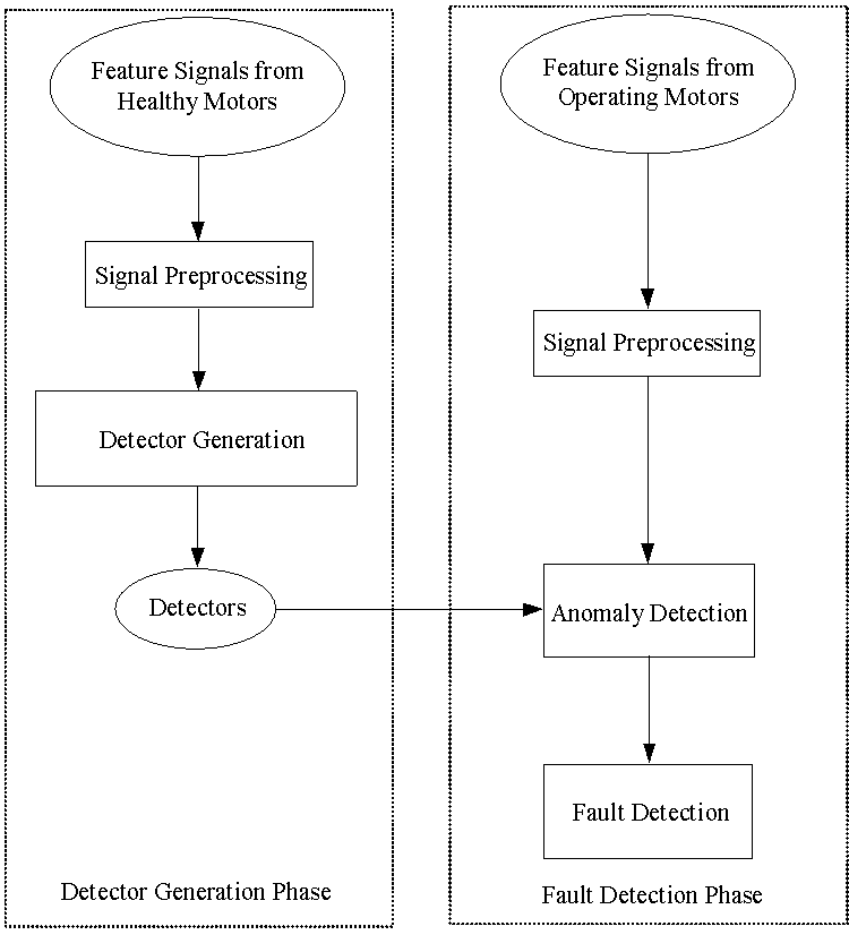

FIGURE 4. Negative Selection Algorithm (NSA) in motor fault detection

the input patterns of the NSA detectors. Secondly, with the negative selection principle, a given number of eligible detectors, S, are generated. Thirdly, the feature signals of the motors under examination are sampled, preprocessed, and matched with these detectors.

Fault detection results can be obtained based on the statistics of the *activated* detectors. A detector is considered activated, if $E < 0$. For the feature signals from the working motors, the numbers of both incorrectly activated detectors and correctly activated ones, A and B, are counted. The quantitative performance criterion, fault detection rate η, is defined:

$$\eta = \frac{B}{A+B} \times 100\%. \tag{3}$$

We must emphasize that the proposed motor fault detection technique is independent of any motors and faults, and can, thus, be a general-purpose solution to a large variety of fault detection problems.

4. **Negative Selection Algorithm (NSA) in Motor Fault Diagnosis.** Motor fault diagnosis generally consists of two principal phases. The first step is to detect the existence of any incipient faults, and the second stage targets at identifying the correct kinds of the faults that have been detected. Inspired by the above idea, we propose a two-level NSA-based motor fault diagnosis scheme, as shown in Figure 5, in this section. The NSA detectors are first used to find out if there are any motor faults occurring. Based on the further analysis of the characteristics of the activated NSA detectors, the motor faults detected can be next classified into different types.

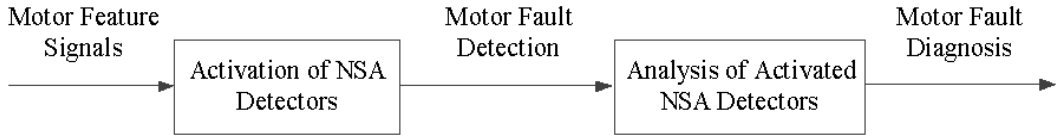

FIGURE 5. Hierarchical NSA-based motor fault diagnosis scheme

Actually, the first stage of the motor fault detection has been described and explained in Section 3. In the NSA-based motor fault diagnosis stage, as shown in Figure 6, the activated detectors are analyzed so as to properly classify the faults already previously detected. There are two main phases involved here: detector training and motor fault classification. In the detector training phase, suppose there are a total of S detectors generated, and K kinds of motor faults to be classified. The numbers of the activation of each detector for every fault is first counted and recorded, which can be denoted as N_i^j ($i = 1, 2, \cdots, K$ and $j = 1, 2, \cdots, S$). For Fault i, all the activated detectors are ranked according to N_i^j. However, to avoid unnecessarily complicated computation, we only select the top M_i, e.g., $M_i = S \times 20\%$, detectors among them to be the 'characteristics detectors' of Fault i. Each characteristics detector is also assigned with a fault diagnosis weight w_i^k as follows:

$$w_i^k = \frac{N_i^j}{\sum_{j=1}^{M_i} N_i^j}, \quad i = 1, 2, \cdots, K \text{ and } k = 1, 2, \cdots, M_i. \tag{4}$$

Obviously, those characteristics detectors with higher values of w_i^k have more impact on the fault diagnosis results. We emphasize that the selection of the characteristics detectors and calculation of the fault diagnosis weights depend on the motor fault data available. In other words, a representative set of motor faults and their corresponding feature signals must be collected off-line in advance and applied in the training of the NSA detectors. In the motor fault diagnosis phase, for the incoming feature signals from the operating motors under inspection, the activation status of the NSA detectors is first examined. Those activated detectors are then matched with the characteristics detectors

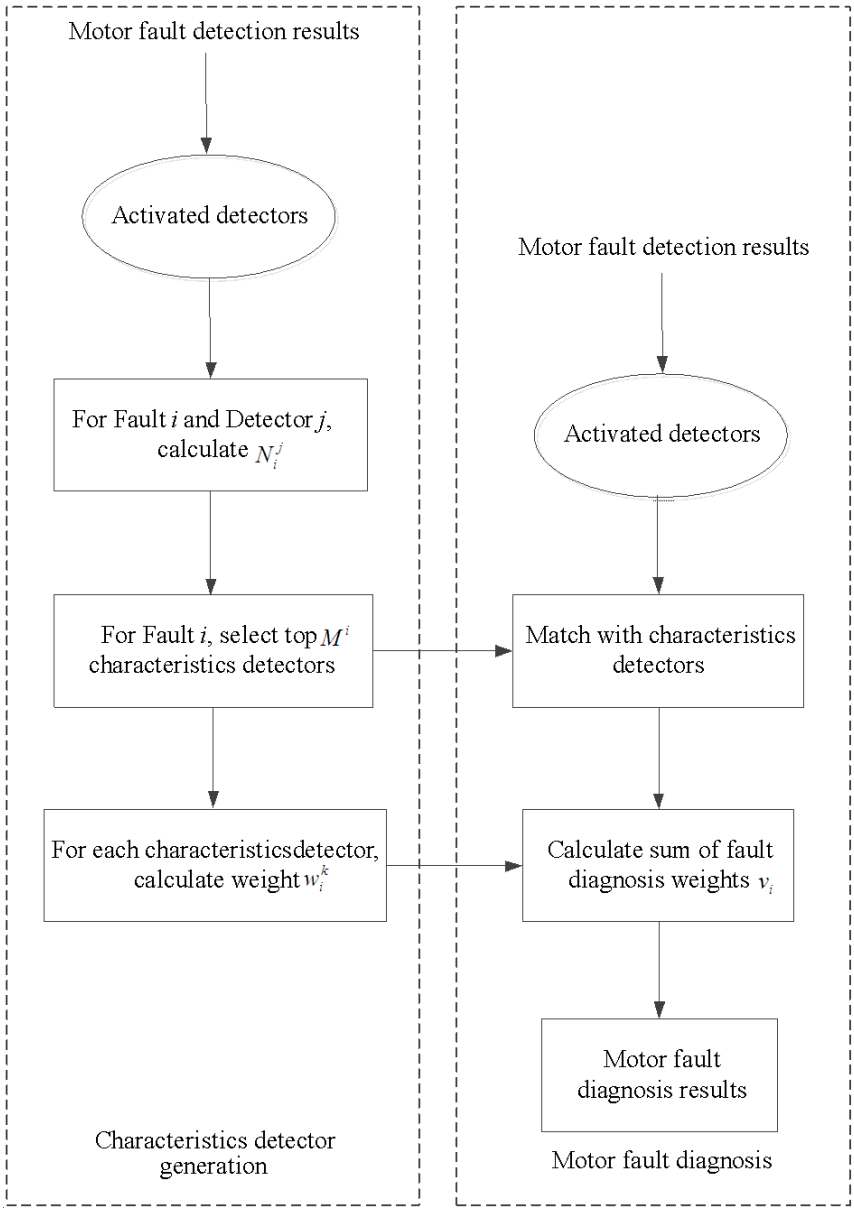

FIGURE 6. NSA-based motor fault diagnosis stage

of each fault, and the fault diagnosis results can be obtained on the basis of the weights of the matched detectors. For example, suppose for Fault i, there are L_i matched detectors. The fault diagnosis weights of this fault w_i^k are added together in order to get v_i:

$$v_i = \sum_{k=1}^{L_i} w_i^k, \quad i = 1, 2, \cdots, K. \tag{5}$$

All the v_i $(i = 1, 2, \cdots, K)$ are calculated and compared with each other, and the fault corresponding to the largest value of v_i will therefore be identified to yield the motor fault diagnosis result.

Our hierarchical NSA-based motor fault diagnosis scheme has a few distinguishing features. Firstly, with a two-level structure, both the fault detection and fault diagnosis results can be simultaneously obtained. Secondly, different from the conventional model-based fault detection approaches, it does not require the domain information of the motor faults to be detected. Lastly, the computational complexity of our solution including

the generation and training of the NSA detectors as well as matching between the NSA detectors and feature time series signals is rather low, which makes it a suitable candidate for time-critical applications. In the next section, the effectiveness of the proposed NSA-based motor fault detection and diagnosis method will be empirically verified using several case studies in computer simulations.

5. **Simulations.** In this section, we investigate our NSA-based fault detection and diagnosis schemes with a few numerical examples.

A. Motor rotor and stator fault detection using the NSA. The validity of the proposed NSA-based motor fault detection scheme is first examined using the faults of rotor and stator. As we know that appropriate monitoring of the working conditions of the motors is important in maintaining their normal status. Thus, a typical fault example of broken rotor and stator is investigated in our simulations. Nevertheless, it should be pointed out that the present paper does not aim at building any real-world motor fault detection and diagnosis systems. All the fault detection and diagnosis problems are deployed here only as representative *testbeds*, and to simplify the presentation, most of the relevant technical details are not considered.

In this motor fault detection case study, the feature signals are the stator current from the healthy motor as well as faulty ones with existing defects on the rotor and stator. These time series signals are shown in Figures 7(a)-7(c), respectively.

There are totally 10,000 samples collected in the above feature signals. All the time series have been split into sliding windows with the width of ten, i.e., $L = 10$, after data preprocessing. The overlapping width between two neighboring windows is one. The number of the NSA detectors generated is $S = 100$, and the fault detection threshold λ of the detectors is $\lambda = 310$. These simulation parameters are usually determined based on experiments. That is to say, they can be solely chosen on the basis of *trial and error*, because of their application dependent characteristics. There is no analytic way yet to choose the best values. For example, large λ may increase the generalization of the NSA detectors but can reduce their sensitivity to the occurrence of incipient faults. Particularly, the healthy stator current signals are divided into two different parts, and each part has 500 sliding windows. The first part is deployed to generate the NSA detectors only, and the second part together with 1,000 sliding windows (500 from rotor fault and 500 from stator fault) extracted from the faulty feature signals are for exploring the fault detection performance of our NSA detectors.

The fault detection rate is calculated based on the numbers of the activated NSA detectors, as given in (3). In the numerical simulations, the numbers of the detectors activated by the fresh healthy feature signal as well as feature signals from the faulty rotor and stator are illustrated in Figures 8(a)-8(c), respectively. The fault detection results obtained are provided in Table 1. It can be concluded that satisfactory detection performances are achieved for both the rotor and stator faults. Note that generation of the NSA detectors in our scheme is independent of the types of the motor faults. In other words, we do not need any background information of the faults to be detected in advance. This unique property is indeed useful under the circumstances, where such knowledge is difficult if not impossible to acquire.

TABLE 1. Detection results of rotor and stator faults

	A	B	η
Rotor Fault	11	84	88.42%
Stator Fault	11	76	87.36%

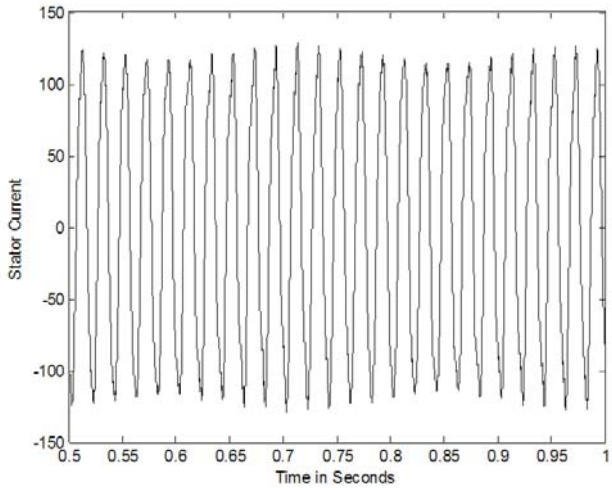

(a) Healthy motor

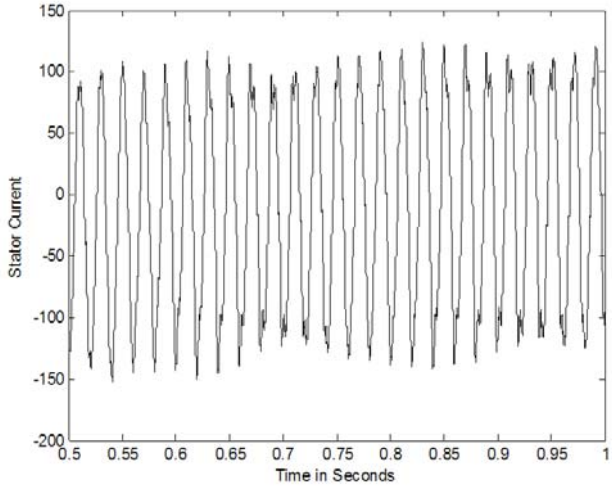

(b) Faulty motor with broken rotor

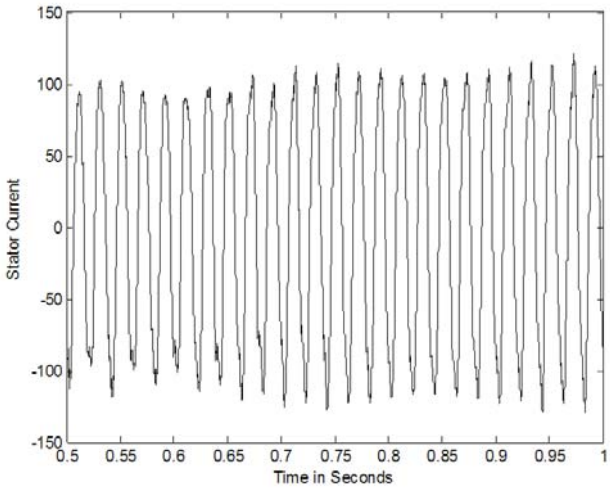

(c) Faulty motor with broken stator

FIGURE 7. Stator current signals of healthy and faulty motors

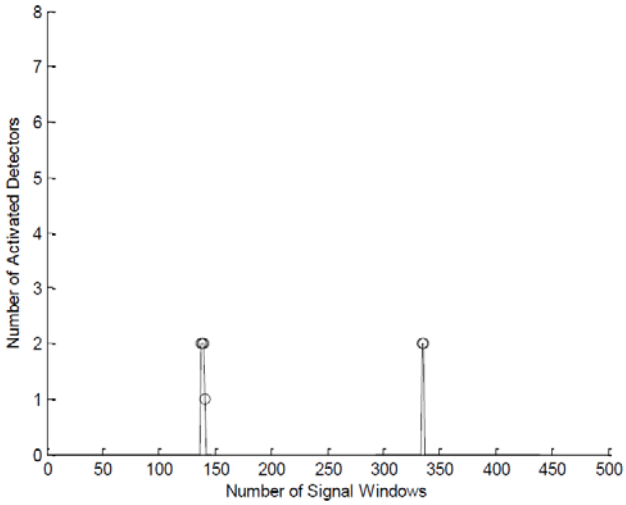

(a) Activated detectors for healthy motor

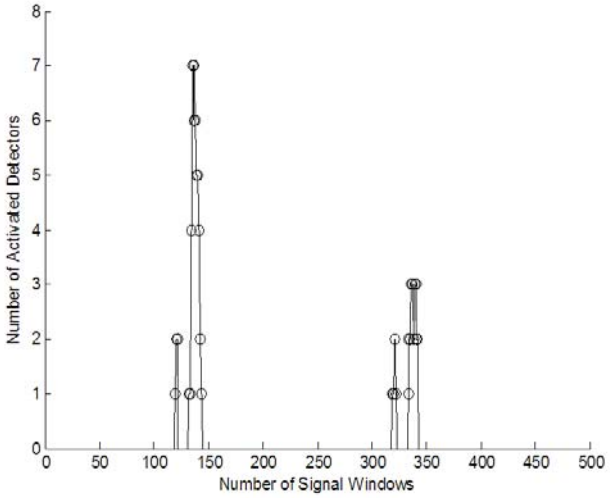

(b) Activated detectors for faulty rotor

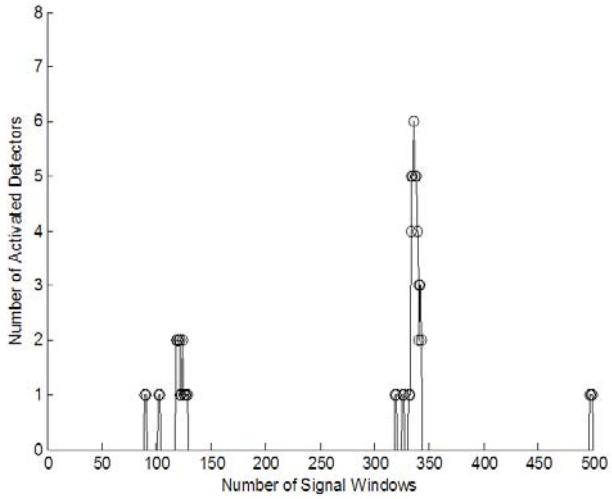

(c) Activated detectors for faulty stator

FIGURE 8. Numbers of activated NSA detectors

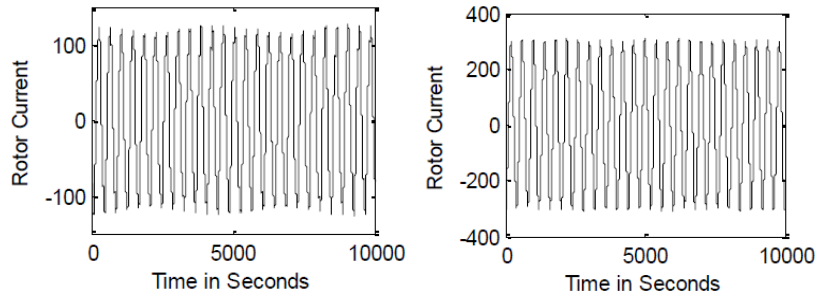

(a) Healthy motor with load C (b) Healthy motor with load O

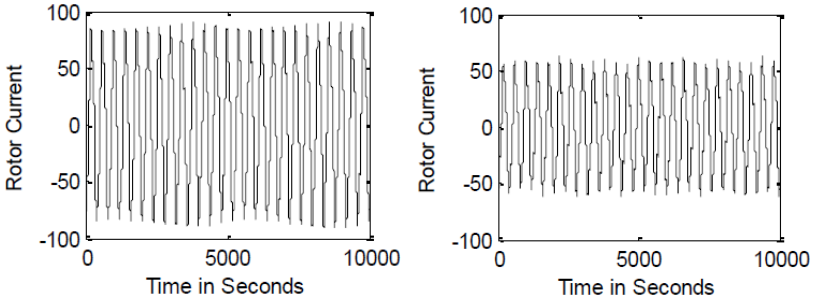

(c) Healthy motor with load S (d) Healthy motor with load U

FIGURE 9. Current signals of healthy motor with four different loads

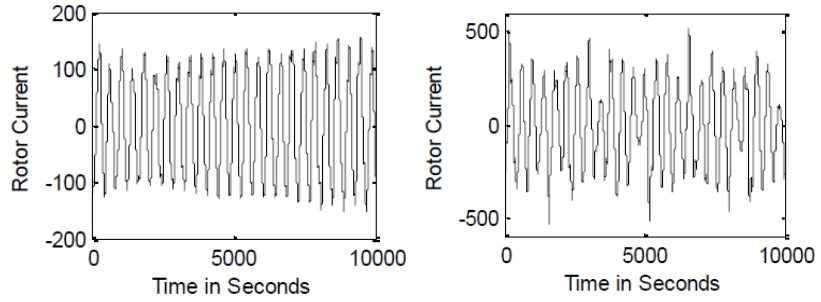

(a) Faulty motor with load C (b) Faulty motor with load O

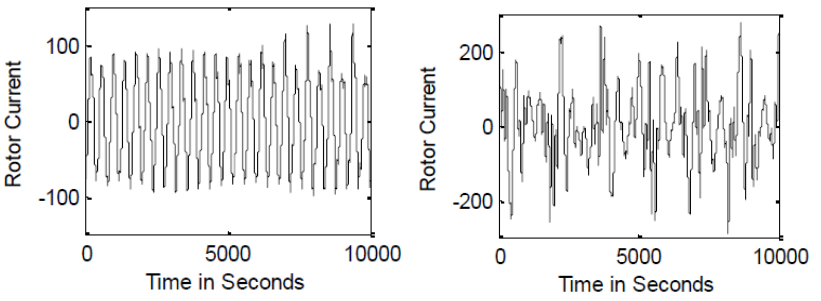

(c) Faulty motor with load S (d) Faulty motor with load U

FIGURE 10. Current signals of faulty motor (rotor fault) with four different loads

It is well known that industrial motors often operate with changing loads in practice. The loads can have a significant impact on the dynamical characteristics of the motors, making our fault detection task even more difficult than the above case of fixed loads. Therefore, the NSA-based fault detection scheme is also investigated for the detection of the motor faults with variant loads. The rotor current signals of a healthy motor loaded with four typical loads are shown in Figures 9(a)-9(d). These loads, namely C, O, S and

U, can cover the full load range of this running motor. Obviously, both the amplitudes and shapes of the current waveforms are affected by the different loads. We only use the rotor fault as an example. The currents of the faulty motor with the rotor fault under the different four loads are illustrated in Figures 10(a)-10(d).

As discussed above, in the data preprocessing stage of our NSA-based motor fault detection scheme, the feature signals from the motors need to be preprocessed. Since the amplitudes of both the healthy and faulty time series are heavily dependent on the motor loads, we have to not only split them into sliding windows (as aforementioned) but also normalize them. More precisely, the above feature signals are normalized so that they can fall into the range of $[-1, 1]$. Each 10,000-sample time series in Figure 9 should be normalized separately. As a matter of fact, the normalization is a crucial preprocessing step to guarantee the successful generation of all the NSA detectors.

Due to the feature signal normalization, the detector threshold is set to be 2.575 this time. A total of 1,000 NSA detectors are generated. The numbers of the activated detectors for the healthy and faulty motors with four different loads are shown in Figures 11 and 12, respectively. The corresponding fault detection results are summarized in Table 2. We can observe that although moderately acceptable fault detection rates can still be achieved, they significantly vary according to the existing motor loads as well. For example, from Table 2, the detection rates under the loads of C and O are much higher than that under the loads of S and U. Thus, how these working loads can influence the performance of our NSA-based motor fault detection scheme is an interesting issue to be explored.

B. NSA-based fault detection in mobile robots. Mobile robots have been widely employed in modern industry. It is well known that the practical terrain for the mobile robots

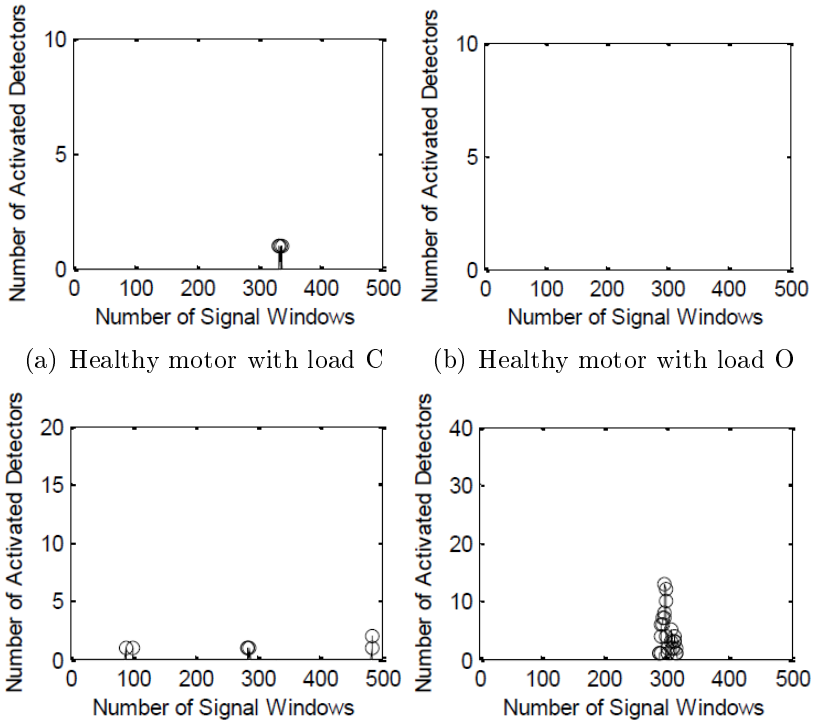

(a) Healthy motor with load C (b) Healthy motor with load O

(c) Healthy motor with load S (d) Healthy motor with load U

FIGURE 11. Numbers of activated NSA detectors for healthy motor

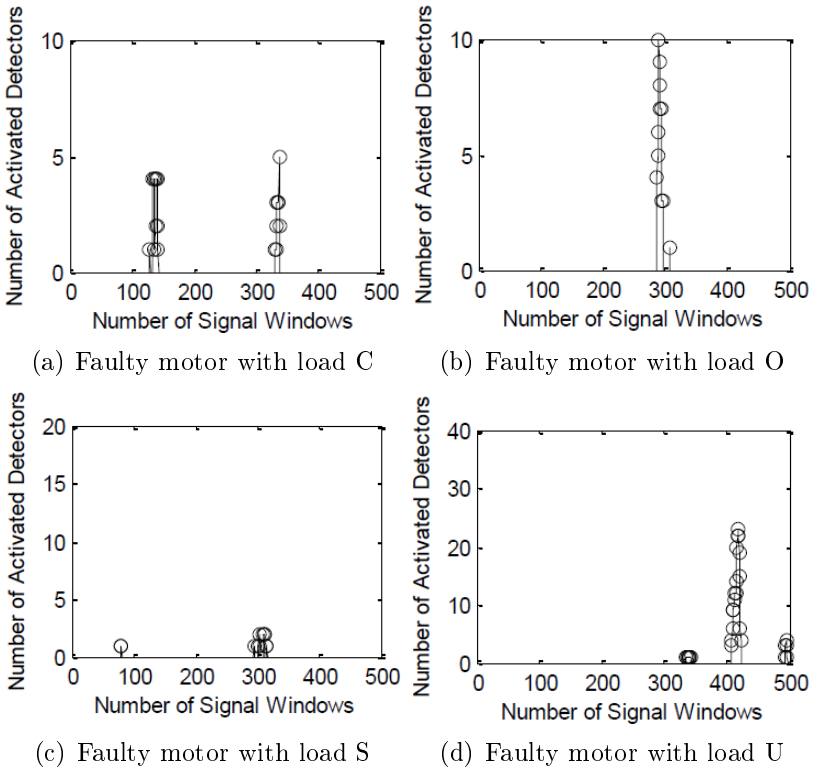

(a) Faulty motor with load C (b) Faulty motor with load O

(c) Faulty motor with load S (d) Faulty motor with load U

FIGURE 12. Numbers of activated NSA detectors for faulty motor

TABLE 2. Fault detection rates of faulty motors with different loads

	A	B	η
Fault C	4	47	92.16%
Fault O	0	63	100%
Fault S	8	15	65.22%
Fault U	109	230	67.85%

is usually rough or rugged. One of the most important requirements for the mission-oriented mobile robots is to have the ability to adapt to various missions, e.g., different payloads, terrains, sizes, and stability margins. Reconfiguration is an efficient approach for designing the mobile robots that meet these requirements. The geometrical trafficability is the basic character of a mobile robot, including the static stability, the height of center of gravity, the clearance, wheelbase and wheel stance, etc. As the static stability is a fundamental metric to describe the geometrical trafficability, calculation of the static stability is necessary. A reconfigurable wheeled mobile robot has been developed with alternative size and trafficability metrics to adapt to uneven terrain [22,23]. Its chassis length and height, caster and camber of the wheels, longitudinal and lateral length of the chassis can be adjusted or changed to obtain different stability and maneuverability. The essential variables of our reconfigurable mobile robot together with their values used here are explained in Table 3 [24]. The isometric view of the prototype of the mobile robot with coordinates system in the four wheels is shown in Figures 13(a)-13(c). Unfortunately, many practical factors, e.g., severe working conditions and aging, can cause incipient faults in the mobile robots. How to efficiently detect these faults at the early stage is undoubtedly important in maintaining their healthy status.

TABLE 3. Parameters of mobile robot prototypes and their values

Parameters	Values	Parameters	Values
distance from centre of wheel longitudinal pivot (m)	0.238	radius of wheel r (m)	0.110
distance from mass centre of steering assembly to longitudinal	0.138	mass of rocker arm distance m_{ar} (kg)	1.0
distance from longitudinal pivot to latitudinal pivot h_0 (m)	0.035	mass of steering assembly m_{st} (kg)	2.8
distance from mass centre of chassis box to differential pivot	0.111	mass of wheel of robot m_w (kg)	4.43
distance from bottom of chassis box to differential pivot h_{x1} (m)	0.161	mass of chassis box m_{box} (kg)	15.6
mass of wheel mechanism m_{wp} (kg)	8.23	caster of front wheel and rear	-12-28
mass of robot m (kg)	48.5	front wheel camber and rear wheel β_f,	-12-28
variable distance from differential pivot to latitudinal pivot h (m)	0.0368 to 0.1035	variable length of wheel base l (m)	0.52 to 0.658

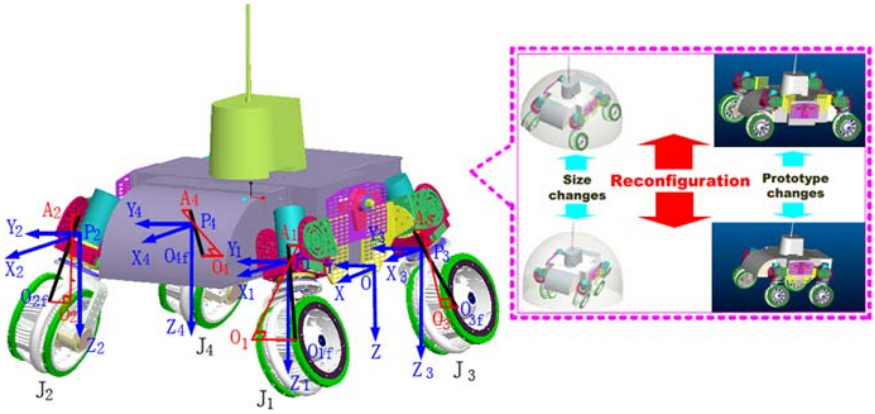

(a)

(b) (c)

FIGURE 13. Isometric view of mobile robot prototype with coordinates system

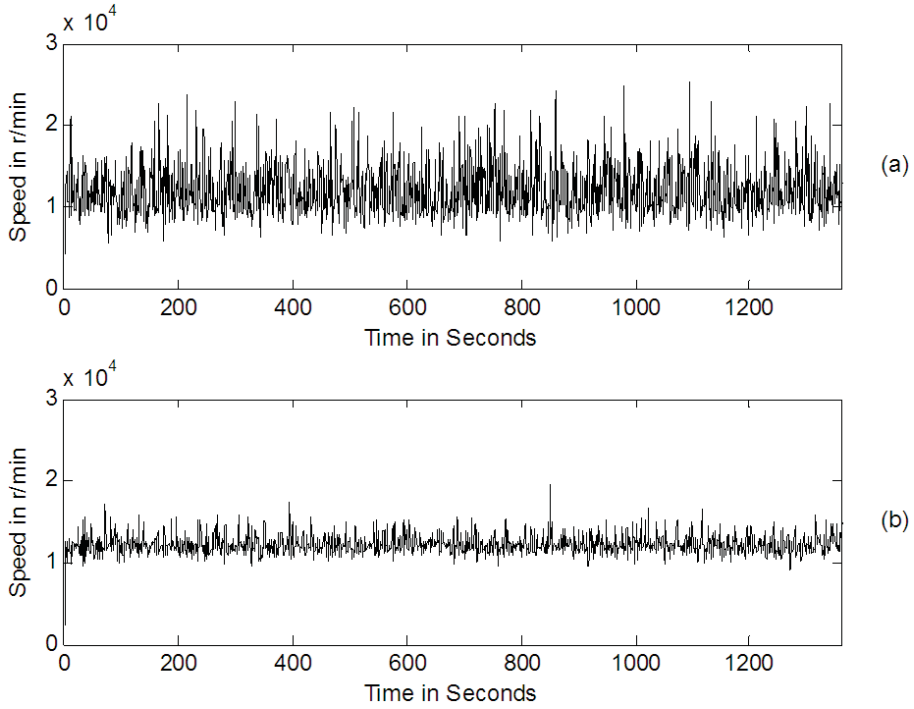

FIGURE 14. Speed signals of healthy and faulty mobile robots in straightforward movement mode on sand ground: (a) healthy mobile robot, (b) faulty mobile robot with broken wheel no. 1

A representative broken wheel fault of the mobile robots is investigated in our simulations. In this mobile robot fault detection case study, the feature signals are collected from the wheel speeds of the reconfigurable mobile robot with four wheels explained above, when the mobile robot is in the straightforward movement mode on the sand ground. Figures 14(a) and 14(b) show the wheel speed signals from a healthy mobile robot as well as a faulty one with the broken wheel no. 1, respectively.

The number of these feature signal samples deployed is around 1,500, and the number of the NSA detectors to be generated is $S = 100$. The fault detection threshold λ is $\lambda = 3 \times 10^4$. As aforementioned, all the time series have been split into non-overlapping windows with the width of ten, i.e., $L = 10$, after data preprocessing. Particularly, the healthy speed signals are divided into two different parts with 500 samples (50 signal windows) each. The first part is deployed to generate the NSA detectors, and the second part together with 500 samples extracted from the faulty speed signals are for exploring the fault detection performance of the detectors generated.

In the simulations, the numbers of the detectors activated by the fresh healthy and faulty speed signals are illustrated in Figures 15(a) and 15(b), respectively. For these activated detectors, we obtain $A = 24$ and $B = 292$. Thus, from (3), the fault detection rate η is calculated to be 92.4%.

The same NSA-based fault detection configuration is also used for detecting the broken wheel fault in other movement modes of the mobile robot on the sand ground. As an illustrative example, the speed signals of the healthy and faulty mobile robots in the self-turning movement mode are demonstrated in Figures 16(a) and 16(b), respectively.

The fault detection results acquired are summarized in Table 4. Apparently, the fault detection rates for our mobile robot are fairly high. However, as we can observe, the difficulty of detecting this broken wheel fault heavily depends on the movement modes of the mobile robot. From Table 4, it is easiest to detect the fault when the mobile robot is in

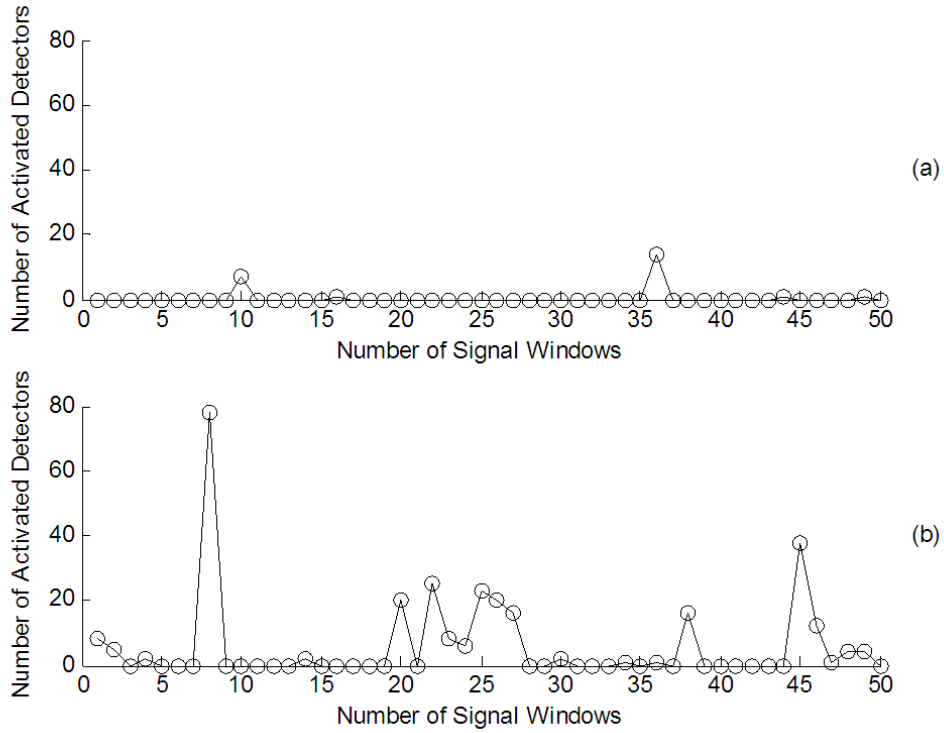

FIGURE 15. Numbers of activated NSA detectors: (a) activated detectors from healthy speed signal, (b) activated detectors from faulty speed signal

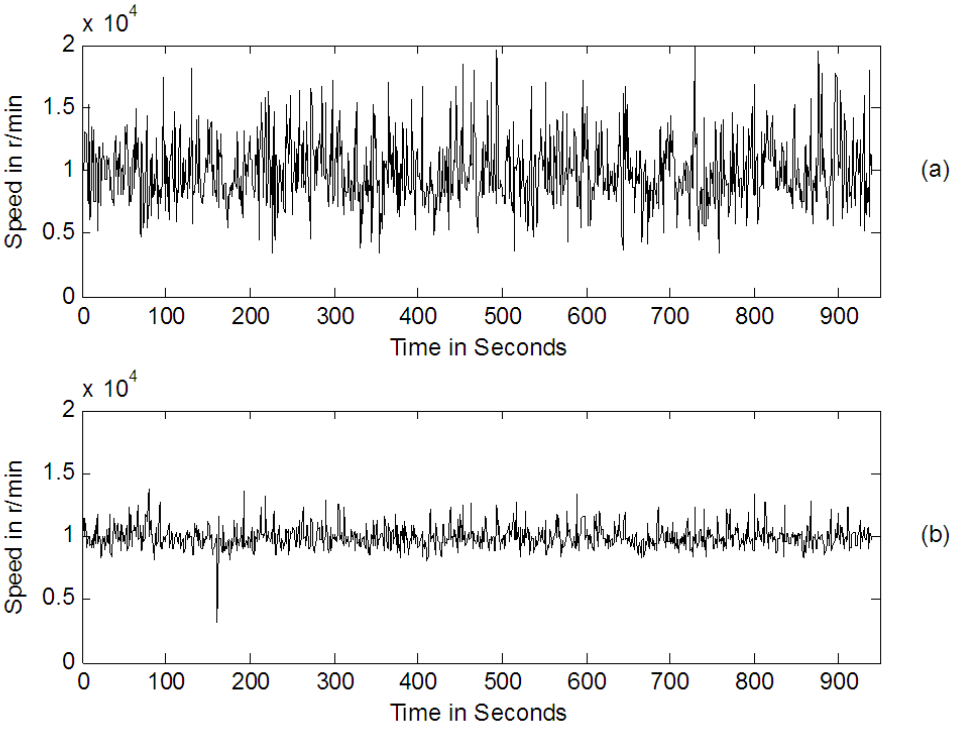

FIGURE 16. Speed signals of healthy and faulty mobile robots in self-turning movement mode on sand ground: (a) healthy mobile robot, (b) faulty mobile robot with broken wheel no. 1

TABLE 4. Fault detection rates of mobile robots in different movement modes on sand ground

Movement Modes	A	B	η
Straightforward	24	292	92.4%
Self-turning	59	381	86.6%
Self-turning Mobile with Speed Difference	20	1440	98.6%
Self-turning with Speed Difference	41	268	86.7%
Single Akarman Mobile	0	3933	100%
Dual Akarman Mobile	1	632	99.8%

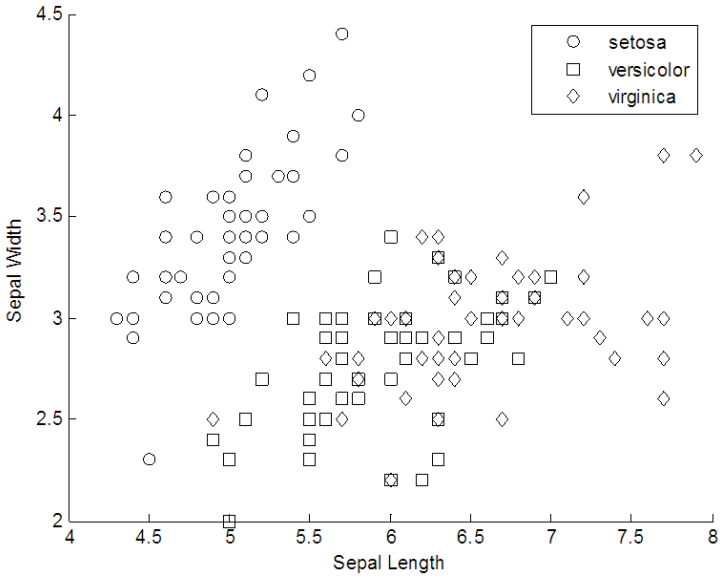

FIGURE 17. Distribution of Fisher's iris data in sepal length-sepal width dimensions

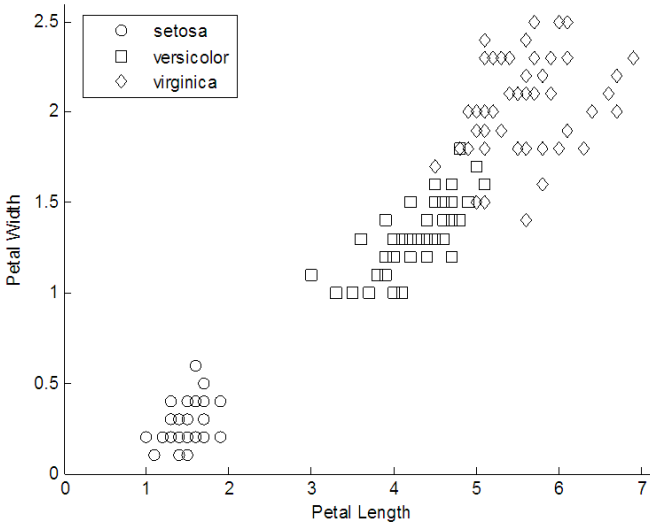

FIGURE 18. Distribution of Fisher's iris data in petal length-petal width dimensions

the single Akarman movement mode, while fault detection in the self-turning movement mode is the most challenging task among the six movement modes.

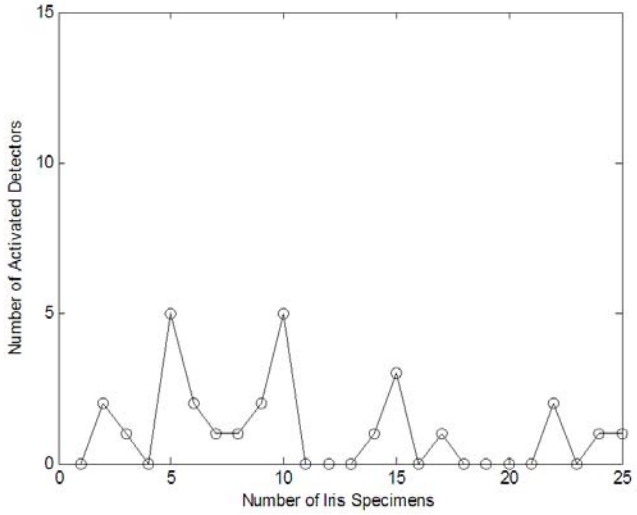

(a) Activated detectors for Setosa

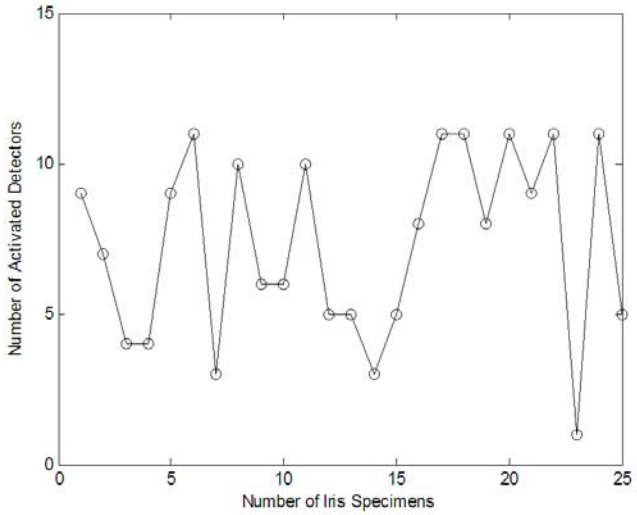

(b) Activated detectors for Virginica

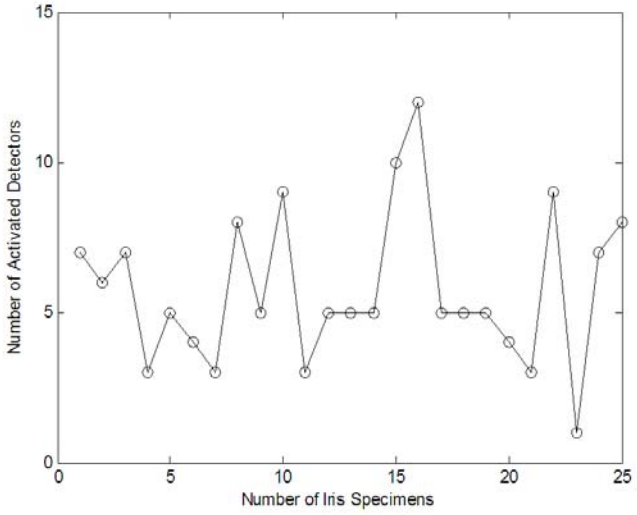

(c) Activated detectors for Versicolor

FIGURE 19. Numbers of activated NSA detectors

C. NSA-based anomaly detection and classification in Fisher's iris data. Fisher's iris data is a well-known benchmark for pattern classification and clustering methods [25,26]. Four attributes, i.e., sepal length, sepal width, petal length, and petal width, of a total of 50 iris specimens are measured from each of the three species: Setosa, Versicolor and Virginica. Figures 17 and 18 illustrate the distributions of Fisher's iris data in the sepal length-sepal width and petal length-petal width dimensions, respectively.

To validate the proposed NSA-based fault detection/diagnosis scheme, we here consider Setosa as the normal samples, and the other two species, Virginica and Versicolor, anomalies. Thus, the effectiveness of the NSA detectors can be examined by the detection and classification of the Virginica and Versicolor species. In our simulations, the number of the detectors employed is 1,000, and the detector radius $r = 0.6$. The specimens of each of the three species are divided into two equal parts. The beginning 25 specimens of Setosa are first used to generate the NSA detectors. The numbers of the activated detectors for Setosa, Virginica and Versicolor are illustrated in Figures 19(a)-19(c), respectively. The anomaly detection results of Virginica and Versicolor are given in Table 5. Apparently, the anomaly detection rates of these two anomalous species are 86.73% and 83.72%, respectively.

Furthermore, the first 25 specimens of Virginica and Versicolor are employed to train their characteristics detectors for classification. The 10 characteristics detectors with classification weights are selected and shown in Tables 6 and 7, respectively. The classification performances of the characteristics detectors are investigated using the remaining 25 specimens. Tables 8 and 9 demonstrate the activated detectors of Virginica and Versicolor, respectively, and the classification results are provided in Table 10. More precisely, for the classification of Virginica from Versicolor, there is 0.9237 *vs.* 0, and for the classification of Versicolor from Virginica, we get 0.8261 *vs.* 0. Therefore, it is found out that our NSA detectors can not only detect the anomaly of Virginica and Versicolor, but also successfully classify these two species.

D. NSA-based motor fault diagnosis. (1) Motor rotor and stator fault diagnosis. In this case study, the NSA-based motor fault diagnosis scheme is applied to classify two different kinds of motor faults: rotor fault and stator fault. The feature signals are measured from the current of the healthy motors and faulty motors (with two faults) with existing

TABLE 5. Anomaly detection of Virginica and Versicolor in Fisher's iris data

	A	B	η
Virginica	28	183	86.73%
Versicolor	28	144	83.72%

TABLE 6. Characteristics detectors of Virginica with classification weights

Detectors	984	305	512	535	692	228	374	783	79	252
Weights	0.1271	0.1186	0.1186	0.1102	0.1102	0.0932	0.0847	0.0847	0.0763	0.0763

TABLE 7. Characteristics detectors of Versicolor with classification weights

Detectors	419	82	609	239	490	570	324	530	542	654
Weights	0.1594	0.1449	0.1449	0.1304	0.1014	0.0870	0.0580	0.0580	0.0580	0.0580

TABLE 8. Activated detectors of Virginica

Detectors	984	305	512	692	535	374	228	252	783	575

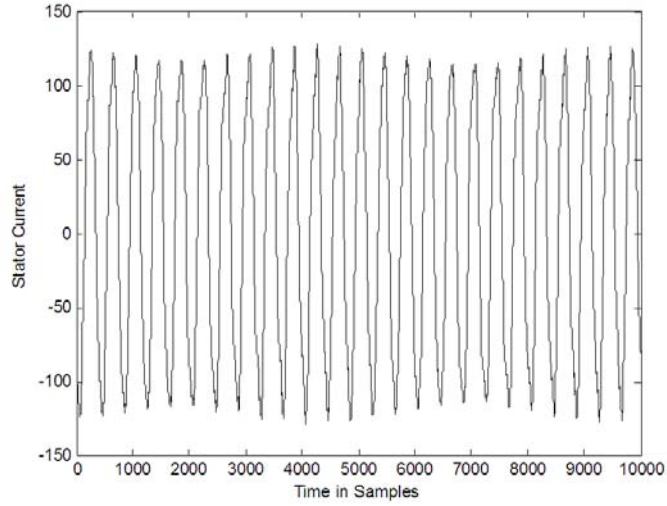

(a) Healthy motor

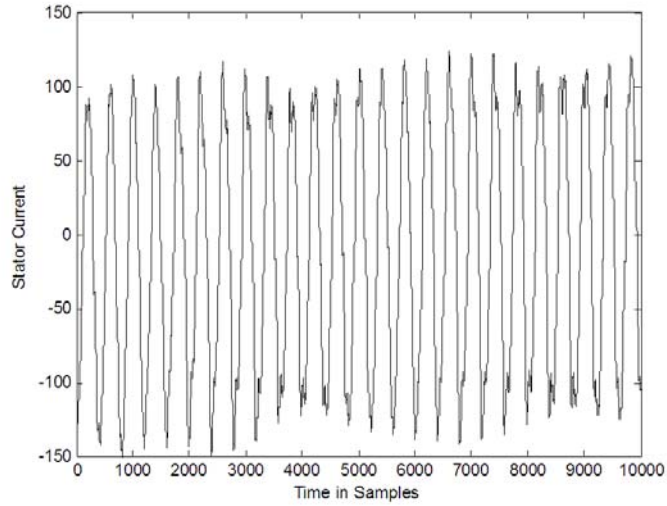

(b) Faulty motor with broken rotor

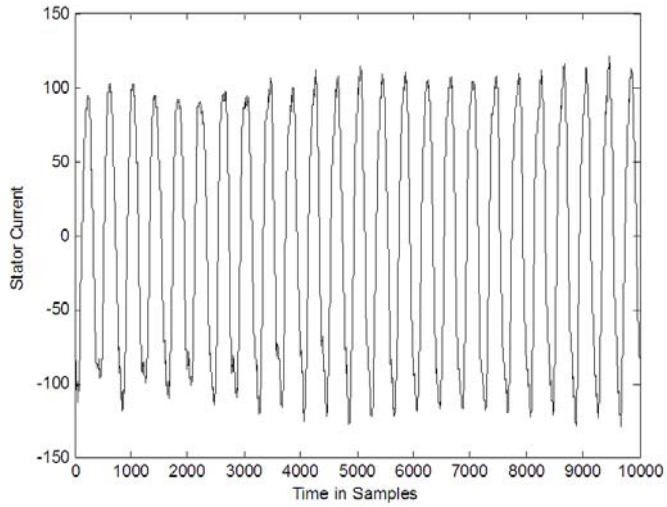

(c) Faulty motor with broken stator

FIGURE 20. Stator current signals of healthy and faulty motors

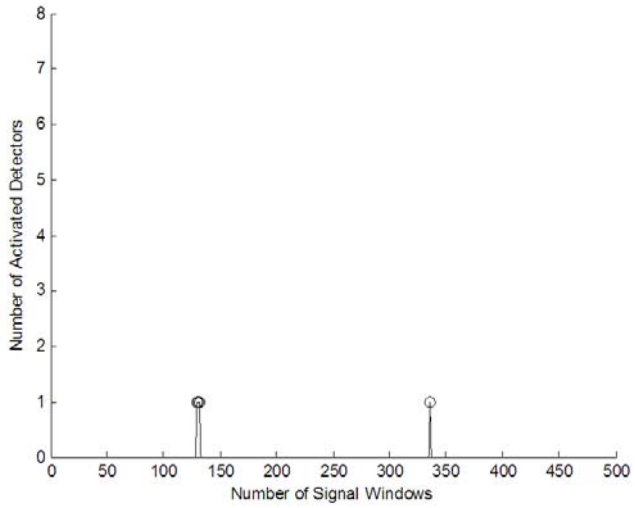

(a) Activated detectors for healthy motor

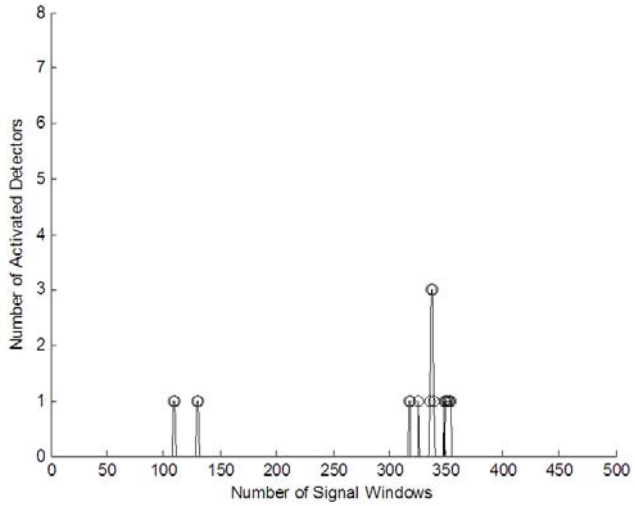

(b) Activated detectors for faulty rotor

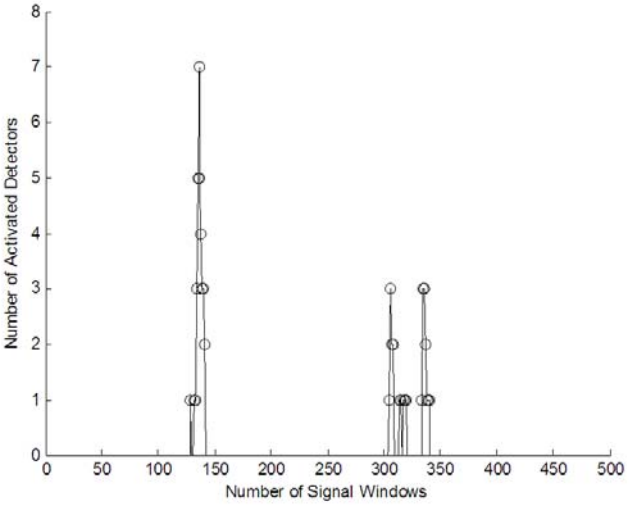

(c) Activated detectors for faulty stator

FIGURE 21. Numbers of activated NSA detectors

TABLE 9. Activated detectors of Versicolor

Detectors	239	419	609	570	82	530	944	838	413	490

TABLE 10. Classification results of Virginica and Versicolor

	v_1	v_2
Virginica	**0.9237**	0
Versicolor	0	**0.8261**

TABLE 11. Detection results of rotor and stator faults

	A	B	η
Rotor Fault	15	162	91.53%
Stator Fault	15	193	92.79%

TABLE 12. Characteristics detectors of rotor fault with fault diagnosis weights

Detectors	214	517	934	88	153	156	356	820	664	679
Weights	0.1296	0.0926	0.0926	0.0741	0.0556	0.0556	0.0556	0.0556	0.0370	0.0370
Detectors	744	795	888	907	935	988	75	155	242	306
Weights	0.0370	0.0370	0.0370	0.0370	0.0370	0.0370	0.0185	0.0185	0.0185	0.0185

defects on the rotor and stator. These time series signals are shown in Figures 20(a)-20(c), respectively.

There are totally 10,000 samples collected in the above feature signals. Again, all the time series have been split into sliding windows with $L = 10$ after data preprocessing. The overlapping width between two neighboring windows is one. The number of the NSA detectors to be generated is $S = 1,000$, and the matching threshold λ of the detectors is $\lambda = 320$. Note that these parameters may considerably affect the fault detection and diagnosis performances, such as robustness to noisy feature signals. Similarly, the healthy current signals are divided into two different parts, and each part has 4,000 signal windows. The first part is deployed to generate the NSA detectors only, and the second part (fresh healthy feature signals) together with 4,000 sliding windows extracted from the faulty feature signals are used for exploring the fault detection & diagnosis capabilities of our NSA-based scheme.

In the motor fault detection phase, the numbers of the detectors activated by the fresh healthy and faulty feature signals from the broken rotor and stator (only the beginning 500 sliding windows) are illustrated in Figures 21(a)-21(c), respectively. The fault detection results obtained are given in Table 11. It can be concluded that reasonable detection performances with the fault detection rates of 91.53% and 78.26% has been respectively achieved for the rotor and stator faults.

In the motor fault diagnosis phase, both the two faults have the same numbers of characteristics detectors, i.e., $M_1 = M_2 = 20$. Like in the preprocessing of the healthy feature signals used in the fault detection stage, the faulty feature signals are also divided into two parts: the first part is employed to train the characteristics detectors, and the second part is for examining the fault diagnosis capability of the proposed scheme. The characteristics detectors together with the fault diagnosis weights of the rotor and stator faults are selected, calculated, and given in Tables 12 and 13, respectively. Note that the characteristics detectors have been numbered, and Table 13 does not show those

TABLE 13. Characteristics detectors of stator fault with fault diagnosis weights

Detectors	888	75	837	507	155	311	214	119	359	934	993
Weights	0.1884	0.1594	0.1449	0.1304	0.1014	0.1014	0.0870	0.0290	0.0290	0.0145	0.0145

TABLE 14. Activated detectors of rotor fault

Detectors	214	744	17	896	795	935	993	298	777	934
Detectors	119	242	243	542	753	345	737	951	102	384

TABLE 15. Activated detectors of stator fault

Detectors	214	311	507	737	934	741	847	517	888	75
Detectors	637	935	242	611	659	837	962	94	277	306

TABLE 16. Fault diagnosis results of rotor and stator faults

	v_1	v_2
Rotor Fault	**0.9855**	0.7778
Stator Fault	0.5507	**0.6481**

detectors of the stator fault after the 11^{th} one, because their fault diagnosis weights are all zeros. Tables 14 and 15 respectively provide the activated detectors of the rotor and stator faults. The fault diagnosis results acquired are summarized in Table 16. As we can observe that when $v_1 = 0.9855 > v_2 = 0.7778$, the rotor fault is identified, and when $v_2 = 0.6481 > v_1 = 0.5507$, the fault detected is classified to be the stator fault. Apparently, both the two faults have been correctly classified. In other words, our scheme is well capable of yielding a good motor fault diagnosis performance.

(2) Motor bearings fault diagnosis. Bearings are indispensable components in rotating machinery. Therefore, appropriate monitoring of their conditions is crucial to guarantee the normal operation of motors [27]. Since the defects on the inner raceway, outer raceway, as well as balls are typical faults of bearings, we will examine the proposed motor fault diagnosis scheme using these three faults in our simulations. Two illustrative examples of the bearings fault are provided in Figures 22(a) and 22(b).

The feature signals are collected from a vibration sensor mounted on top of the eight-ball bearings with a motor rotation speed at 1,782 rpm. Figures 23(a)-23(d) show the vibration signal samples from the healthy bearings and those faulty bearings with the inner raceway, outer raceway, and ball faults, respectively.

The relevant simulation parameters in the generation of the NSA detectors are given as follows:

number of feature signal samples used: 20,000,
number of detectors: $S = 5,000$,
window width: $N = 10$,
matching threshold: $\lambda = 0.0775$.

There are a total of 20,000 new samples in each of the three verification time series. The beginning 10,000 samples are taken from healthy bearings, and the following 10,000 samples are from three faulty bearings with the corresponding inner race, outer raceway, and ball faults. The fault detection performances of our detectors for the inner raceway, outer raceway, and ball faults are verified and illustrated in Figures 24(b)-24(d), respectively. The detection rates of the NSA detectors for the above three different bearings

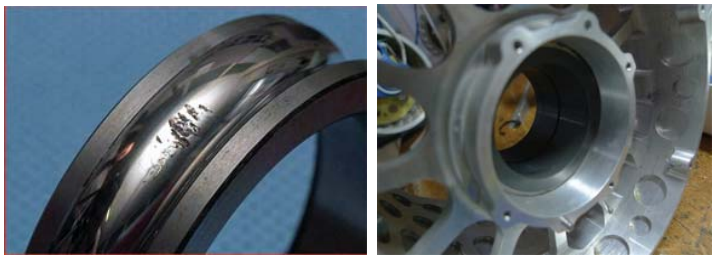

(a) (b)

FIGURE 22. Two illustrative examples of bearings fault

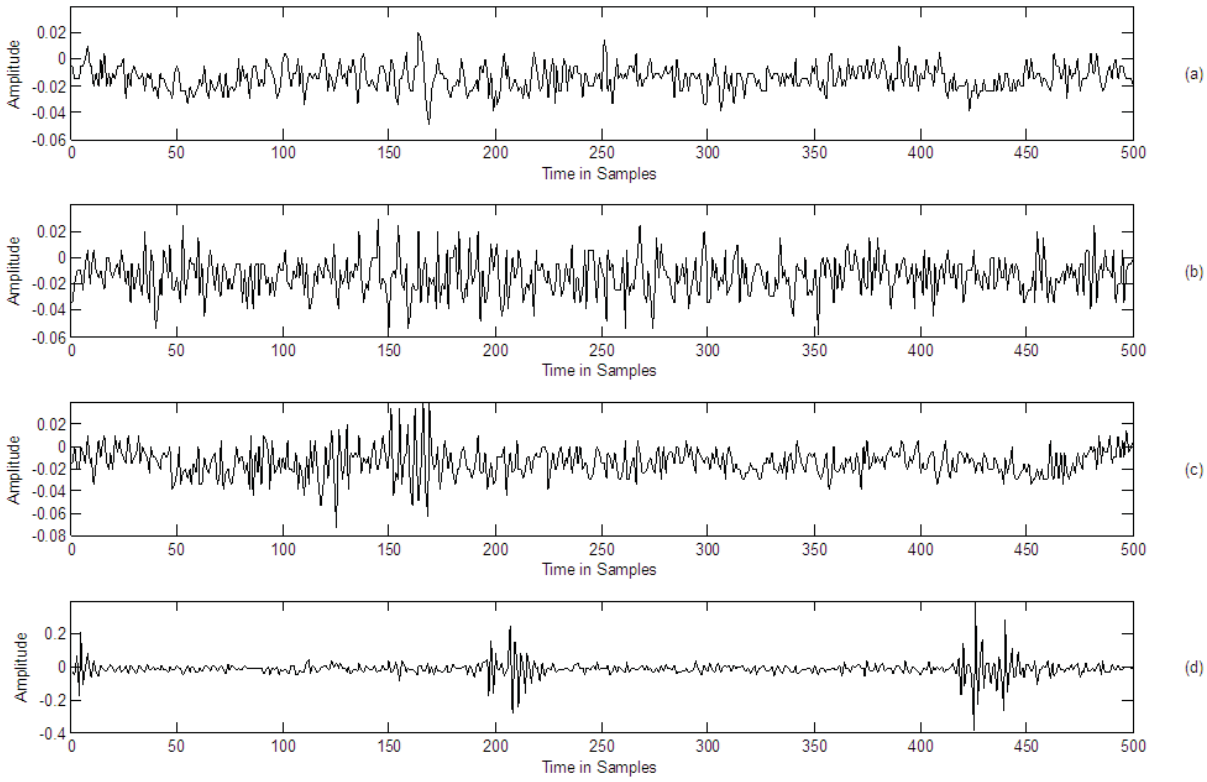

FIGURE 23. Features signals of healthy and faulty bearings: (a) healthy bearings, (b) faulty bearings with inner raceway fault, (c) faulty bearings with outer raceway fault, (d) faulty bearings with ball fault

TABLE 17. Fault detection rates of NSA detectors

	A	B	η
Inner Raceway Fault	64	534	89.3%
Outer Raceway Fault	64	425	86.91%
Ball Fault	64	1368	95.53%

faults are summarized in Table 17. As we can see from Table 17, the fault detection rates of the inner raceway, outer raceway, and ball faults are 89.3%, 86.91% and 95.53%, respectively. That is to say, the NSA-based motor fault detection stage is well capable of achieving an acceptable fault detection performance.

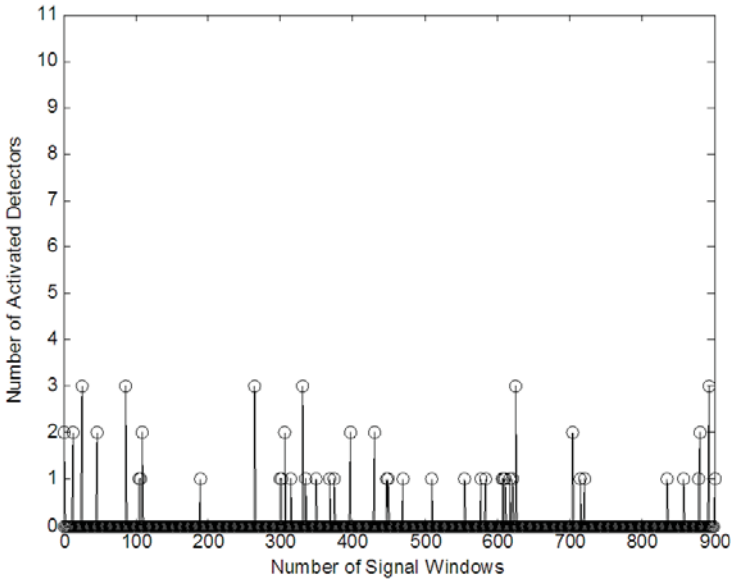

(a) Activated detectors for healthy bearings

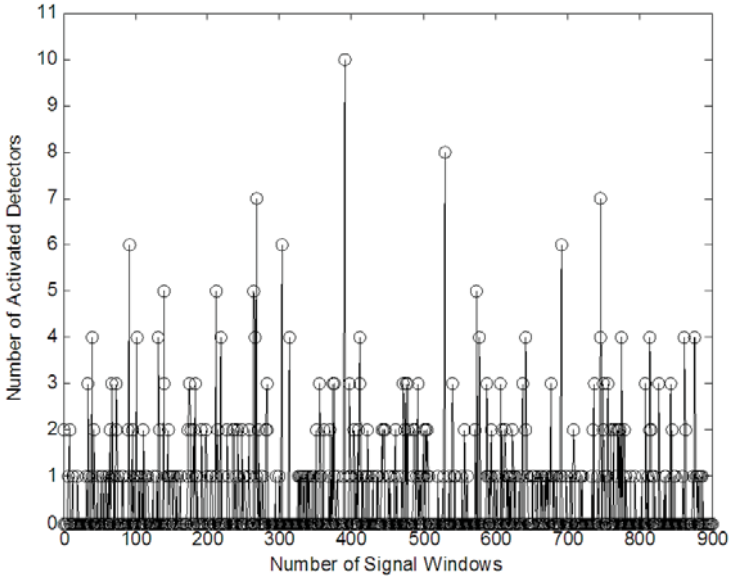

(b) Activated detectors for inner raceway fault

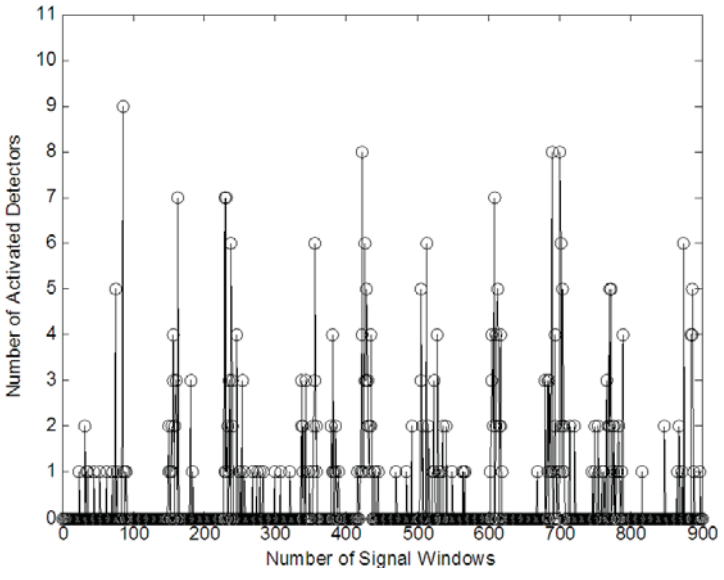

(c) Activated detectors for outer raceway fault

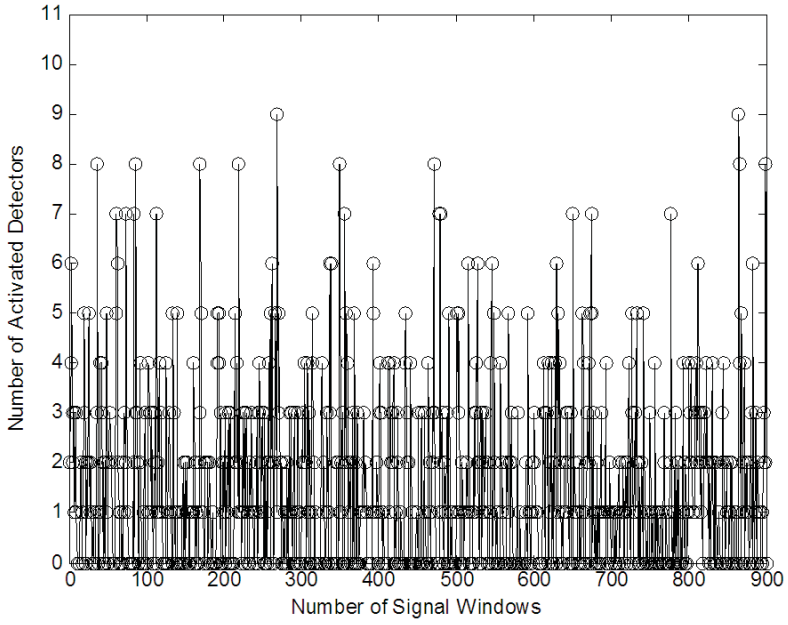

(d) Activated detectors for ball fault

FIGURE 24. Numbers of activated NSA detectors

TABLE 18. Top 10 characteristics detectors of inner raceway fault with fault diagnosis weights

Detectors	3257	3784	4408	395	3752	987	530	2598	4305	4431
Weights	0.0407	0.0378	0.0291	0.0262	0.0262	0.0233	0.0203	0.0203	0.0203	0.0203

TABLE 19. Top 10 characteristics detectors of outer raceway fault with fault diagnosis weights

Detectors	2598	3257	1823	3784	2886	395	1773	1244	4348	105
Weights	0.0373	0.0313	0.0254	0.0239	0.0239	0.0239	0.0209	0.0179	0.0179	0.0164

TABLE 20. Top 10 characteristics detectors of ball fault with fault diagnosis weights

Detectors	2598	3257	4305	1244	2516	3784	987	4281	4348	898
Weights	0.0620	0.0388	0.0349	0.0349	0.0271	0.0233	0.0233	0.0194	0.0194	0.0155

TABLE 21. Top 10 activated detectors of inner raceway fault

Detectors	3257	395	2598	2857	3238	4408	3444	4348	105	1627

TABLE 22. Top 10 activated detectors of outer raceway fault

Detectors	2598	1696	1823	3257	1244	395	987	2516	2886	3819

TABLE 23. Top 10 activated detectors of ball fault

Detectors	2598	4305	987	1244	2516	2759	4281	1415	1619	3257

TABLE 24. Fault diagnosis results of motor bearings faults

	v_1	v_2	v_3
Inner Raceway Fault	**0.7035**	0.5775	0.6537
Outer Raceway Fault	0.5262	**0.6047**	0.5701
Ball Fault	0.6599	0.6744	**0.7552**

In the motor fault diagnosis phase, the numbers of the characteristics detectors for the three bearings faults are all chosen to be 100, i.e., $M_1 = M_2 = M_3 = 100$. To simplify our presentation here, only the top 10 characteristics detectors and their fault diagnosis weights of the inner raceway, outer raceway, and ball faults are shown in Tables 18-20, respectively. Tables 21-23 demonstrate the top 10 activated detectors of these three faults. The fault diagnosis results are provided in Table 24. Obviously, for the diagnosis of the inner raceway fault, we have $v_1 = 0.7035 > v_3 = 0.6537 > v_2 = 0.5775$, and for the outer raceway fault, there is $v_2 = 0.6047 > v_3 = 0.5701 > v_1 = 0.5262$. From $v_3 = 0.7552 > v_2 = 0.6744 > v_1 = 0.6599$, the ball fault is identified from the other two faults. Therefore, we can conclude that all the three bearings faults have been correctly classified. The proposed NSA-based motor fault detection and diagnosis scheme is indeed effective and flexible in coping with multiple fault detection and diagnosis problems.

6. **Conclusions.** In this paper, a novel NSA-based motor fault detection and diagnosis scheme is presented and discussed. The proposed approach has a unique hierarchical structure, in which the motor faults can be detected and identified in the first and second stages, respectively. The Fisher's iris data classification problem and three practical motor fault diagnosis examples including a case study of the mobile robot fault detection are used to examine and demonstrate its effectiveness. Different from the conventional motor fault detection solutions, the NSA-based method does not require the availability of any prior fault knowledge beforehand, and only the feature signals from the healthy motors are needed. Note that our scheme is independent of the types of the motors and faults under consideration. That is, it is not only limited to the electric motors, and can be generalized for the fault detection and diagnosis of other kinds of plants, such as power systems, chemical processes, mechanical engineering, and telecommunications networks. In the future work, we are going to further examine the feasibility of this NSA-based motor fault detection and diagnosis method with various sorts of motor faults.

Acknowledgements. This research work was funded by the Academy of Finland under Grants 135225, 127299 and 137837. He Xu's work was supported by the National Science Foundation of China under Grant 60775060, the Natural Science Foundation of the Heilongjiang Province of China under Grant F200801, the Specialized Research Fund for the Doctoral Program of Higher Education under Grants 200802171053 and 20102304110006, and Harbin Science and Technology Innovation Talents Special Fund under Grant 2012RFXXG059. The authors would like to thank the anonymous reviewers for their insightful comments and constructive suggestions that have improved the paper.

REFERENCES

[1] C. A. Janeway, P. Travers, M. Walport and M. Shlomchik, *Immunobiology: The Immune System in Health and Disease*, 5th Edition, Garland Publishing, New York, 2001.

[2] L. N. de. Castro and J. Timmis, *Artificial Immune Systems: A New Computational Intelligence Approach*, Springer-Verlag, London, 2002.

[3] D. Dasgupta, Advances in artificial immune systems, *IEEE Computational Intelligence Magazine*, vol.1, no.4, pp.40-49, 2006.

[4] E. Ulker, NURBS curve fitting using artificial immune system, *International Journal of Innovative Computing, Information and Control*, vol.8, no.4, pp.2875-2888, 2012.
[5] S. Forrest, A. S. Perelson, L. Allen and R. Cherukuri, Self-nonself discrimination in a computer, *Proc. of the IEEE Symposium on Research in Security and Privacy*, Los Alamos, CA, USA, pp.202-212, 1994.
[6] D. Dasgupta and F. González, An immunity-based technique to characterize intrusions in computer networks, *IEEE Transactions on Evolutionary Computation*, vol.6, no.3, pp.281-291, 2002.
[7] D. Dasgupta and S. Forrest, Tool breakage detection in milling operations using a negative selection algorithm, *Technical Report CS95-5*, Department of Computer Science, University of New Mexico, 1995.
[8] D. Dasgupta, K. Krishnakumar, D. Wong and M. Berry, Negative selection algorithm for aircraft fault detection, *Proc. of the 3rd International Conference on Artificial Immune Systems*, Catania, Sicily, Italy, pp.1-13, 2004.
[9] Z. Ji and D. Dasgupta, Revisiting negative selection algorithm, *Evolutionary Computation*, vol.15, no.2, pp.223-251, 2007.
[10] F. González, *A Study of Artificial Immune Systems Applied to Anomaly Detection*, Ph.D. Thesis, Division of Computer Science, University of Memphis, Memphis, 2003.
[11] Z. Ji and D. Dasgupta, Real-valued negative selection algorithm with variable-sized detectors, *Proc. of Conference on Genetic and Evolutionary Computation*, Seattle, WA, USA, pp.287-298, 2004.
[12] Z. Ji, *Negative Selection Algorithms: From the Thymus to V-Detectors*, Ph.D. Thesis, University of Memphis, 2006.
[13] T. Stibor, J. Timmis and C. Eckert, A comparative study of real-valued negative selection to statistical anomaly detection techniques, *Proc. of the International Conference on Artificial Immune Systems*, Banff, AL, Canada, pp.262-275, 2005.
[14] S. Nandi, H. A. Toliyat and X. Li, Condition monitoring and fault diagnosis of electrical motors – A review, *IEEE Transactions on Energy Conversion*, vol.20, no.4, pp.719-729, 2005.
[15] D. Basak, A. Tiwari and S. P. Das, Fault diagnosis and condition monitoring of electrical machines – A review, *Proc. of the IEEE International Conference on Industrial Technology*, Mumbai, India, pp.3061-3066, 2006.
[16] Y. L. Murphey, M. A. Masrur, Z. Chen and B. Zhang, Model-based fault diagnosis in electric drives using machine learning, *IEEE/ASME Transactions on Mechatronics*, vol.11, no.3, pp.290-303, 2006.
[17] S. Kim and H. Bae, Real-time anomaly detection for business process monitoring, *ICIC Express Letters*, vol.6, no.4, pp.1109-1114, 2012.
[18] X. Z. Gao, S. J. Ovaska, X. Wang and M.-Y. Chow, A neural networks-based negative selection algorithm in fault diagnosis, *Neural Computing and Applications*, vol.17, no.1, pp.91-98, 2008.
[19] X. Z. Gao, S. J. Ovaska and X. Wang, A GA-based negative selection algorithm, *International Journal of Innovative Computing, Information and Control*, vol.4, no.4, pp.971-979, 2008.
[20] X. Z. Gao, S. J. Ovaska, X. Wang and M.-Y. Chow, Clonal optimization-based negative selection algorithm with applications in motor fault detection, *Neural Computing and Applications*, vol.18, no.7, pp.719-729, 2009.
[21] X. Z. Gao, S. J. Ovaska, X. Wang and M.-Y. Chow, Multi-level optimization of negative selection algorithm detectors with application in motor fault detection, *International Journal of Intelligent Automation and Soft Computing*, vol.15, no.3, pp.353-375, 2010.
[22] C. Liu, X. Wei and J. Yang, A path planning method based on improved genetic algorithm for mobile robot in static environment, *ICIC Express Letters*, vol.5, no.12, pp.4283-4290, 2011.
[23] H. Xu, Z. Zhang, D. Tan, X. Z. Gao, G. Peng and S. Yu, Optimization of mobile robot based on projection method and harmony search, *Proc. of the 2008 IEEE International Conference on Robotics and Biomimetics*, Bangkok, Thailand, pp.1653-1658, 2009.
[24] H. Xu, Z. Zhang, K. Alipour, K. Xue and X. Z. Gao, Prototypes selection by multi-objective optimal design: Application to a reconfigurable robot in sandy terrain, *Industrial Robot*, vol.38, no.6, pp.599-613, 2011.
[25] R. A. Fisher, The use of multiple measurements in taxonomic problems, *Annals of Eugenics*, vol.7, pp.179-188, 1936.
[26] *Fisher's Iris Data*, ftp://ftp.ics.uci.edu/pub/machine-learning-databases/iris/.
[27] B. Li, M.-Y. Chow, Y. Tipsuwan and J. C. Hung, Neural-network-based motor rolling bearing fault diagnosis, *IEEE Transactions on Industrial Electronics*, vol.47, no.5, pp.1060-1069, 2000.